ISSN (Print) 1226-1750
ISSN (Online) 2233-6656
Journal of Magnetics 22(4), 610-616 (2017) https://doi.org/10.4283/JMAG.2017.22.4.610

A Novel Tunable Dual-band Left-Handed Metamaterial

Si Li[1], Atef Z. Elsherbeni[2], Wenhua Yu[3], Wenxing Li[1]*, and Yunlong Mao[1]

[1]College of Communication and Information Engineering, Harbin Engineering University, Harbin, Heilongjiang, China
[2]Electrical Engineering Department, Colorado School of Mines, Golden, CO, 80401, USA
[3]2COMU, INC. Fairfax, VA 22030, USA

(Received 7 October 2017, Received in final form 27 November 2017, Accepted 27 November 2017)

In this paper, we propose a novel tunable left-handed metamaterial (LHM), the capacitor-loaded short wire pairs (CL-SWPs). It is composed of a pair of short wires connected through a variable capacitor. This LHM is single-sided, and it exhibits not only tunable negative permeability, but also a wide band negative permittivity. It is pointed out with theoretical analysis that its left-handed performance is related to the mutual coupling coefficient. A tunable dual-band LHM is also proposed by simply adding a double slits split ring resonator to this LHM. The simulated results indicate that the closer the two LH bands are, the better performance the CL-SWP related left-handed band is, hence identifying our theoretical analysis. The proposed structure is geometrically simple, low-cost and easy for fabrication, and it can be used as a basic particle in the design of tunable multi-band LHMs.

Keywords : dual-band, left-handed metamaterials, tunability

1. Introduction

Left-handed Metamaterials (LHMs) are materials that have negative permeability (μ) and permittivity (ε). LHMs can be implemented with arrayed metallic wires or electric resonators together with magnetic resonators [1-4]. Because of the intrinsic and narrow resonance frequency band of most LHMs, it cannot be used in some wide operating frequency areas [5].

Some tunable LHMs have been proposed by using various additional materials or structures, such as the ferrites [6-11], liquid crystals [12-14], varactors [15-17], and tunable structures [18-20]. Ferrites or liquid crystals can be easily added to conventional LHMs to achieve tunability. In [10], a ferrite rod is simply added to a LHM composed of split ring resonators (SRRs) and metallic wires. In [12], the liquid crystal is simply inserted between two Omega-type resonators. Such kinds of LHMs are easy to design, but have the disadvantages such that ferrites based tunability requires big magnetic bias, and liquid crystals based tunability has a finite tunable range [5]. Tunable structures can be implemented with the displacement between layers [20], the change of the thickness of the substrate [19]. This kind of tunability is not as convient or flexible as the previous ones, but much easier to be used in practice. Varactors loaded tunability has been used in microwave engineering applications since they can be easily integrated into microwave circuits. However, the insertion requires a proper gap region, which increases the design difficulties.

Even though these LHMs are tunable, they are still not sufficient to meet the increasing requirements of multi-band applications. Multi-band LHMs could be implemented with simply arranging multiple LHM units together [21, 22], or with particular elements that contains multiple resonances [23-27]. Such kinds of LHMs are well-designed and usually have complex metallic structures for the purpose of making the μ-negative and the ε-negative frequency ranges overlapped.

In this paper, we propose a novel tunable LHM structure that is composed of variable capacitor loaded short wire pairs (CL-SWPs). Short wire pairs (SWPs) are paralleled metallic wire pairs printed on both sides of the substrate [28-33]. As discussed in [28], the equivalent capacitance of the magnetic resonance of SWPs comes from the coupled metallic wires. With the consideration that variable capacitor can be used instead of this coupling capacitance, we came up with a novel tunable LHM unit where a pair

*Corresponding author: Tel: +86-0451-82519806
Fax: +86-0451-82519806, e-mail: liwenxing@hrbeu.edu.cn

of short wires are vertically located on the same side of a substrate and connected through a variable capacitance. This novel structure exhibits negative permeability at a tunable narrow frequency range but also negative permittivity over a wide frequency range. It is pointed out with theoretical analysis that the magnetic resonance of the proposed structure is closely related to the mutual coupling coefficient. We also implement a novel tunable dual-band LHM by simply adding a double slits split ring resonator to the CL-SWPs. It is seen from the simulated results that the closer the two LH bands are, the stronger the CL-SWP related magnetic resonance is, which verified our theoretical analysis. The implementation of this tunable dual-band LHM also indicates that the proposed novel tunable LHM can serve as a basic particle in the design of tunable multi-band LHMs.

2. Theoretical Analysis

According to the theoretical analysis of the SRRs in [3, 34], the magnetic resonance is motivated by the electromotive force around the circumference of the split rings. The geometry of a unit SRR is illustrated in Fig. 1. Considering an infinite array of such SRRs arranged in three orthogonal directions with a spatial period of d, and an incident magnetic field polarized along the y direction, that is, perpendicular to the SRRs, there would be electromotive force and induced current I along the rings, satisfying:

$$\begin{aligned} \mathrm{EMF} &= j\omega\pi r^2\mu_0 H_0 = RI + I/(-j\omega C) \\ &\quad + (-j\omega L)I + (-j\omega FL)I, \end{aligned} \tag{1}$$

where H_0 is the external magnetic field, R, L, and C are the parasitic resistance, inductance, and capacitance of each ring, respectively, and FL is the mutual inductance between different rings. With $L = \pi r^2\mu_0/d$, and $F = \pi r^2/d^2$, the current I is given as

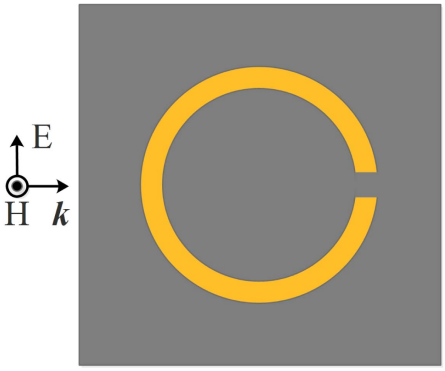

Fig. 1. (Color online) Geometry of a SRR unit.

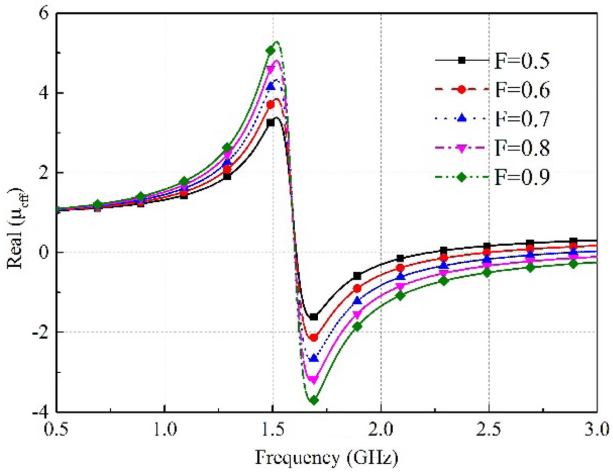

Fig. 2. (Color online) The real part of the effective permeability when R = 1 Ohm, L = 1 nH, and C = 10 pF.

$$I = \frac{-j\omega\pi r^2\mu_0 H_0}{j\omega\pi r^2\mu_0\left[1-\frac{\pi r^2}{d^2}\right]-R+\frac{1}{j\omega C}} = \frac{-dH_0}{\left(1-F-\frac{1}{\omega^2 LC}\right)+\frac{Rj}{\omega L}}. \tag{2}$$

Based on the magnetic moment per unit volume, $M = \pi r^2/I/d^3$ and $\mu_{eff} = (B/\mu_0)/(B/\mu_0 - M)$, B is the corresponding external magnetic flux, then we can obtain the final effective permeability as follows:

$$\mu_{eff} = 1 - \frac{F\left(1-\frac{1}{\omega^2 LC}\right)}{\left(1-\frac{1}{\omega^2 LC}\right)^2+\frac{R^2}{(\omega L)^2}} + j\frac{\frac{R}{\omega L}}{\left(1-\frac{1}{\omega^2 LC}\right)^2+\frac{R^2}{(\omega L)^2}}. \tag{3}$$

From the analysis above, it is obvious that the effective permeability is completely irrelevant to the shape of the magnetic resonators. The real part of μ_{eff} can be negative with proper selections of F, R, L and C, while the imaginary part μ_{eff} will always be positive. For a given structure if we have R = 1 Ohm, L = 1 nH, and C = 10 pF, then the change of the real part of μ_{eff} with F changing from 0.5 to 0.9 is displayed in Fig. 2, where 'Real (μ_{eff})' represents the real part of the effective permeability.

Obviously, the real part of the effective permeability is closely related to F. For a given structure, when F is getting larger, the bandwidth of the negative Real (μ_{eff}) will become wider, and the minimum value for Real (μ_{eff}) will become smaller.

3. Verification Simulation

Based on the theoretical analysis, we simulated a

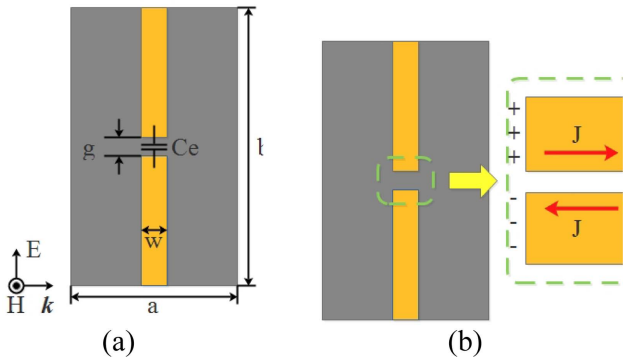

Fig. 3. (Color online) (a) Structure of the proposed LHM. (b) Illustration of current distribution.

Fig. 4. Equivalent circuit for a CL-SWP unit.

variable capacitor-loaded SWPs using HFSS. In Fig. 3, a = 27 mm, b = 54 mm, g = 2.5 mm, and w = 5 mm. The metallic structure is printed on a 1.27 mm-thick Rogers-6006 substrate whose relative permittivity is 6.15. A variable capacitor is used to connect the wires, which reversed the directions of current flows on both sides of the gap, as illustrated in Fig. 3(b). The equivalent circuit is approximated in Fig. 4, where the self-inductance can be calculated using [35]:

$$L = 2\times10^{-4} l\left[\ln\left(\frac{l}{w+t}\right)+1.193+0.2235\frac{w+t}{l}\right] \quad (4)$$

where l is the length of the strip line, w is the width, and t is the thickness. Assume a function 'Cal_ind(l,w,t)' to represent (4), then the equivalent inductance L_e is approximated as:

$$L_e = cal\_ind(b/2, d, t), \quad (5)$$

which is 0.72nH. Hence, the magnetic resonant frequency can be calculated as:

$$f_m = \frac{1}{2\pi\sqrt{L_e C_e}}. \quad (6)$$

When the C_e = 6Pf, f_m = 2.43 GHz; when C_e = 9pF, f_m = 1.99 GHz. And when C_e = 14 pF, f_m= 1.6 GHz.

Simulated S parameters are displayed in Fig. 5, where the solid lines represent S_{11} and the dashed lines represent S_{21}. The capacitance of the loaded capacitor is varying from 6 pF to 14 pF, hence causing the lowest value of S_{11} moving from approximately 2.4 GHz to 1.75 GHz.

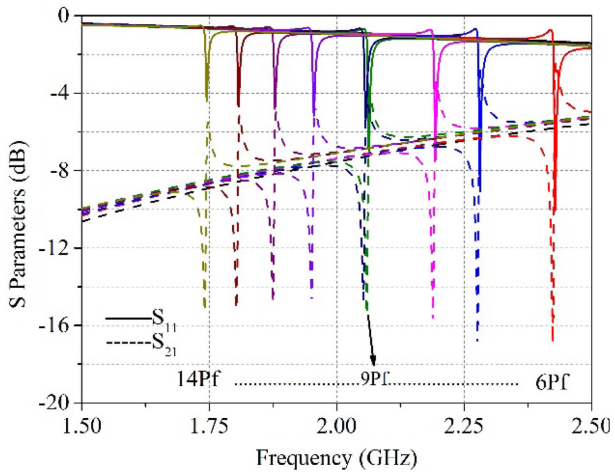

Fig. 5. (Color online) Simulated S parameters with the embedded capacitance ranging from 6 pF to 14 pF. The solid lines represent S_{11}, while dashed lines represent S_{21}, respectively.

The corresponding effective permittivity (ε), permeability (μ), impedance (Z), and refractive index (R), are retrieved using the 'S parameters retrieval method' proposed in [36], and they are displayed with their real part (Real) and imaginary part (Imag) respectively in Fig. 6. In Fig. 6(a),

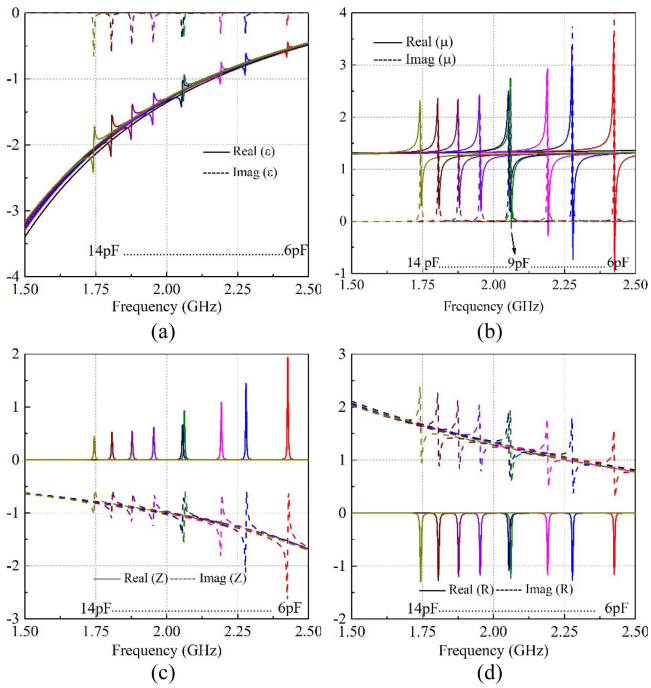

Fig. 6. (Color online) Retrieved effective (a) permittivity ε, (b) permeability μ, (c) impedance Z, and (d) refractive index R, with the embedded capacitance ranging from 6 pF to 14 pF. The solid lines represent the real part while the dashed lines represent the imaginary part, respectively.

even an electric resonance can also be observed with the change of the loaded capacitance, it is not strong enough to affect the polarity of effective permittivity, since the CL-SWPs functions as arrayed metallic wires which exhibits negative permittivity over the discussed frequency range. In Fig. 6(b), negative permeability can only be observed when the loaded capacitance is from 6 pF to 9 pF. In another word, the magnetic resonance is only strong enough to extract negative permeability with these capacitance. It is also observed that the simulated results matches well with the analytic ones. The refractive index is always negative over the discussed frequency range, as illustrated in Fig. 6(d).

Therefore, we successfully implement a single band tunable LHM. It is observed from the simulated results that negative permeability is achieved at a tunable narrow frequency range, while negative permittivity is achieved over the whole discussed frequency range. With respect to the fact that this LHM is single-sided, there is a potential that this structure can serve as a basic particle in the design of tunable multi-band LHM.

4. Dual-band LHM

A double-slits SRRs (DS-SRRs) is chosen here as a magnetic resonator together with the proposed structure to build a tunable dual-band LHM. As is commonly known, DS-SRRs alone are able to extract negative permeability. The geometry of this DS-SRR is displayed in Fig. 7(a), where a = 27 mm, b = 54 mm, e = 6 mm, f = 0.8 mm, r1 = 9 mm, r2 = 12 mm. This SRR is also printed on a 1.27 mm-thick Rogers-6006. Corresponding equivalent circuit is illustrated in Fig. 7(b).

The capacitance of this SRR is calculated as:

$$C_{total} = C_g / 2 + C_s \tag{7}$$

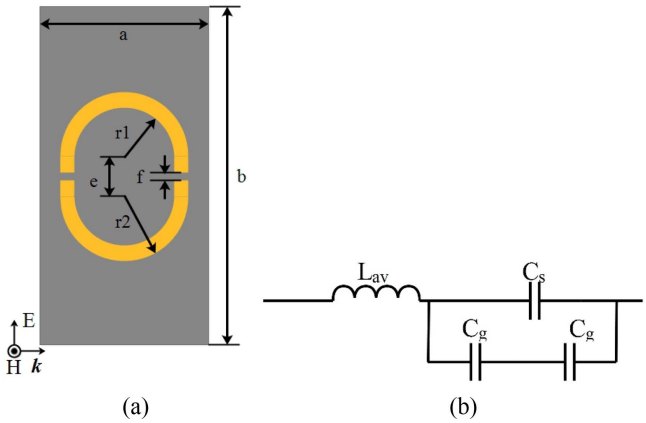

Fig. 7. (Color online) (a) Geometry of the double slits SRR and (b) the corresponding equivalent circuit.

where C_g is the gap capacitance, and C_s is the surface capacitance. According to the transmission line theory [35], for the coplanar strips on a substrate, the capacitance per unit length of two paralleled strip lines are calculated using:

$$C_{pul} = \varepsilon_0 \varepsilon_e F(k) \tag{8}$$

where ε_0 is the permittivity of free space, ε_e and $F(k)$ are calculated as:

$$\varepsilon_e = 1 + (\varepsilon_r - 1) F(k) / 2F(k1) \tag{9}$$

$$F(k) = \begin{cases} \dfrac{1}{\pi} \ln\left(2\dfrac{1+\sqrt{k'}}{1-\sqrt{k'}}\right), & 0 < k \le \dfrac{1}{\sqrt{2}} \\ \pi \ln\left(2\dfrac{1+\sqrt{k}}{1-\sqrt{k}}\right)^{-1}, & \dfrac{1}{\sqrt{2}} < k \le 1 \end{cases} \tag{10}$$

where $k = a/b$, $a = s/2$, $b = w + s/2$, w is the width of the strips, and s is gap width between the strips,

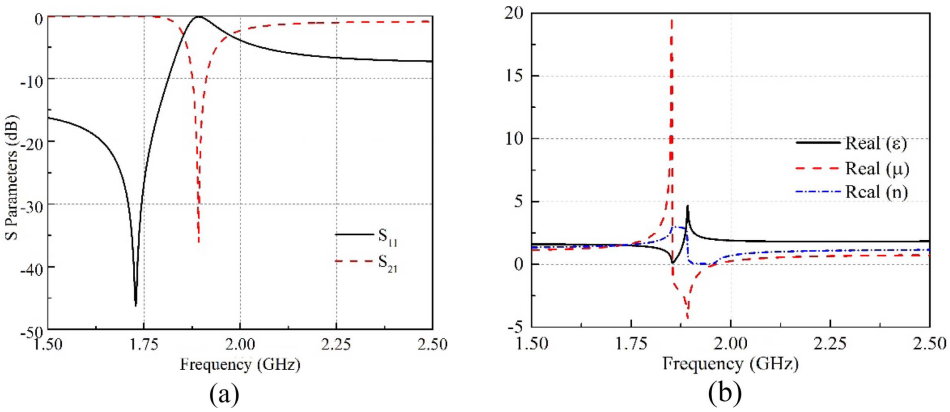

Fig. 8. (Color online) (a) Simulated S parameters (b) the retrieved effective parameters, where 'Real (ε)' is the real part of effective permittivity, 'Real (μ)' is the real part of the effective permeability, and 'Real (n)' is the real part of the refractive index.

$k' = \sqrt{1-k^2}$, and $k1 = \sinh(\pi a/2h)\sinh(\pi b/2h)$. For this double slits SRR, with respect to the estimation method [37], $s = f$, and $w = r1 + (e–f)/2$, hence, C_g is 0.142pf. The calculation for the $C_s = C_{s1} + C_{s2}$ is approximated as [38]:

$$\begin{cases} C_{s1} = \dfrac{\varepsilon_0(t+r2-r1)}{\pi}\left(\log\dfrac{2(r1+r2)}{g}+e-f\right) \\ C_{s2} = \dfrac{\varepsilon_0(\varepsilon_r-1)(t+r2-r1)}{2\pi}\left(\log\dfrac{2(r1+r2)}{g}+e-f\right) \end{cases} \quad (11)$$

where C_{s1} is the surface capacitance through air, while C_{s2} is the surface capacitance through the substrate. Hence, C_s = 0.192pf. The total capacitance C_{total} is 0.264pf.

The total equivalent self-inductance for the double slits SRR can also be approximated using (4), and it can also be approximated as:

$$L_{av} = cal\_indc(r2-r1, \pi(r1+r2)/2+e-f, t), \quad (12)$$

hence, the resonant frequency for the double slits SRR is 1.83 GHz.

The simulated S parameters are displayed in Fig. 8(a). The real part of the retrieved effective parameters are displayed in Fig. 8(b). It is observed that for this DS-SRR, the magnetic resonant frequency is approximately 1.9 GHz, which matches well with our analytic results, and the single negative bandwidth is 0.107 GHz.

For a better demonstration of the dual-band property, we only displayed the simulated S parameters in Fig. 9, and the retrieved effective parameters in Fig. 10, when the loaded capacitance is 10 pF. In these figures, the solid lines represent the real part of the complex values, and the dashed lines represent the imaginary part.

In Fig. 9, there are 3 passing bands. In Fig. 10(a), the real part of the effective permittivity is negative at frequencies lower than 2.2 GHz. In Fig. 10(b), negative permeability can be observed at frequencies from 1.848 GHz to 1.88 GHz, and 2.002 GHz to 2.079 GHz. Hence, the proposed structure is identified as a dual-band LHM with double negative properties at frequencies from 1.848 GHz to 1.88 GHz, and 2.002 GHz to 2.079 GHz. Even though we can't exactly tell which one of the negative permeability frequency band corresponds to the CL-SWP, it is clear that its left-handed transmission character is greatly improved, compared to Fig. 5.

We listed the corresponding resonant frequencies for the single-band CL-SWP LHM and the dual-band LHM (CL-SWP + DS-SRR) with the loaded capacitance tune from 8 pF to 15 pF where significant negative parameters can be observed (Table 1). We also listed the bandwidth and the minimum value of the effective permeability. In this table, 'Fr' refers to the resonant frequency, 'BW' is the absolute bandwidth, and 'MN' refers to the minimum value of the effective permeability.

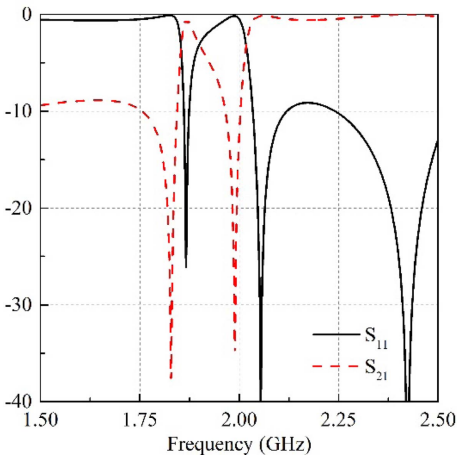

Fig. 9. (Color online) Simulated S parameters in dB when the embedded capacitance is 10 pF. Here, the black solid line represents S_{11}, while the red dashed line represents S_{21}.

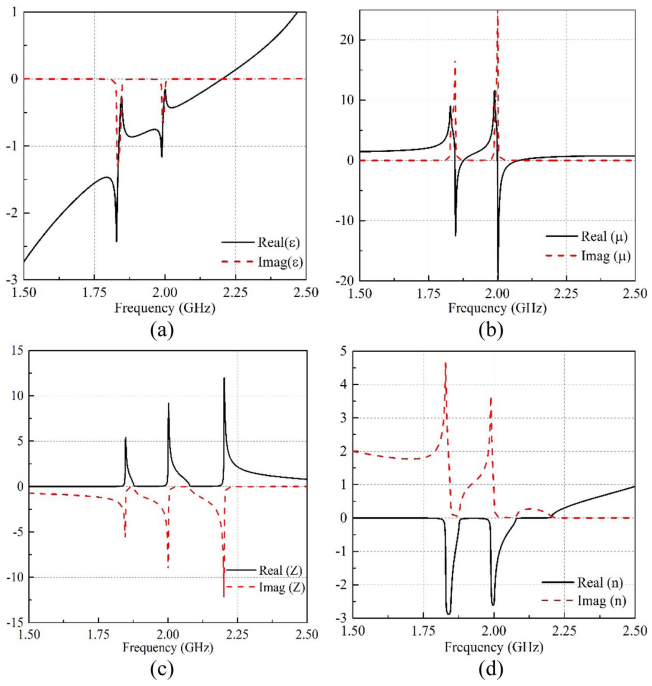

Fig. 10. (Color online) The retrieved effective (a) permittivity, (b) permeability, (c) impedance and (d) refractive index when the embedded capacitance is 10 pF. The solid black lines here represents real part of the parameters, while the red dashed lines represents the imaginary part of the parameters.

Because of the interactions between the CL-SWP and the DS-SRR, both the resonant frequencies for the dual-band LHM are slightly shifted, of which one is always around 1.9 GHz, while the other one shows the same

Table 1. Corresponding resonant frequencies, bandwidth and maximum negative value for the short wire pairs and the dual-band LHM.

Ce (pF)	CL-SWP			CL-SWP + DS-SRR					
				1st LH band			2nd LH band		
	Fr	BW	MN	Fr	BW	MN	Fr	BW	MN
8	2.192	0.002	-0.28	2.149	0.014	-2.909	1.926	0.095	-25.42
9	2.063	0.001	-0.134	2.052	0.05	-11.27	1.899	0.06	-22.00
10	2.056	null	null	1.848	0.032	-12.46	2.002	0.077	-19.71
11	1.954	null	null	1.77	0.016	-7.09	1.983	0.093	-26.62
12	1.879	null	null	1.704	0.012	-4.78	1.97	0.098	-23.46
13	1.807	null	null	1.664	0.011	-3.77	1.935	0.098	-17.89
14	1.746	null	null	1.632	0.01	-2.97	1.904	0.099	-20.14
15	1.546	0.001	-0.128	1.525	0.005	-2	1.957	0.102	-28.29

changing tendency as that of CL-SWP with the changing of the loaded capacitance. Additionally, as listed in Table 1, the minimum negative permeability for the 2nd LH band is smaller than −20 for most *Ce*, while for the 1st LH band, this value is relatively larger. Hence, we may assume that the 1st LH band is related to CL-SWP, while the 2nd LH band is related to DS-SRR.

With this assumption, we can now compare the performance of the CL-SWP for the single-band case (CL-SWP only) and the dual-band case (CL-SWP + DS-SRR). For the sing-band case, when the loaded capacitance is larger than 9 pF and smaller than 15 pF, the effective permeability is positive at a narrow frequency range, while for the dual-band case, negative permeability can be observed at a much wider frequency range. Additionally, the minimum negative permeability for the dual-band case is much smaller. These differences come from the mutual coupling between the CL-SWP and DS-SRR. When the DS-SRR is printed on the other side of the substrate, *F* is greatly increased. As showed in Fig. 2, when *F* is getting larger, the bandwidth extends and the minimum negative permeability decreases. As the CL-SWP related resonant frequency is moving closer to the resonant frequency of DS-SRR, the mutual coupling between them also increases, hence, as listed in the '1st LH band' column, the bandwidth is getting wider and the minimum negative permeability is also getting smaller. All these phenomena match well with Fig. 2.

5. Conclusion

In this paper, we introduced a novel tunable LHM structure that is composed of a pair of short wires connected through a variable capacitor. This structure is not only capable of extracting tunable negative permeability but also negative permittivity over a wide frequency range. With theoretical analysis, we pointed out that its LH performance is closely related to the mutual coupling coefficient. We also implement a tunable dual-band LHM by simply adding a DS-SRR to the proposed LHM. It is indicated from the simulated results that the closer the two LH bands are, the better performance the CL-SWPs related LH band is, hence identifying our theoretical analysis. The proposed structure is geometrically simple, cheap and easy for fabrication, and it can be used as a basic particle in the design of tunable multi-band LHMs.

Acknowledgements

This paper was supported by National Defense "973" Basic Research Development Program of China (no. 6131380101), by Pre-research Fund of the 12th Five-Year Plan (no. 4010403020102 and no. 4010103020103), and the Fundamental Research Funds for the Central Universities (no. HEUCFD1433 and HEUCF1508).

References

[1] R. A. Shelby, D. R. Smith, and S. Schultz, Science **292**, 77 (2001).
[2] D. R. Smith, W. J. Padilla, D. C. Vier, S. C. Nemat-Nasser, and S. Schultz, Phys. Rev. Lett. **84**, 4184 (2000).
[3] J. B. Pendry, A. J. Holden, D. J. Robbins, and W. J. Stewart, IEEE Trans. Microw. Theory Techn. **47**, 2075 (1999).
[4] R. Liu, A. Degiron, J. J. Mock, and D. R. Smith, Appl. Phys. Lett. **90**, 263504 (2007).
[5] J. Zhong, Y. Huang, G. Wen, H. Sun, and W. Zhu, Procedia Eng. **29**, 802 (2012).
[6] B. Du, Z. Xu, J. Wang, and S. Xia, **66**, 21 (2016).
[7] Y. Yong-Jun, H. Yong-Jun, W. Guang-Jun, Z. Jing-Ping, S. Hai-Bin, and O. Gordon, Chin. Phys. B **21**, 038501 (2012).

[8] H. U. Zhen-Yan, Chin. J. Radio **24**, 799 (2009).
[9] P. He, J. Gao, Y. Chen, P. V. Parimi, C. Vittoria, and V. G. Harris, J. Phys. D Appl. Phys. **42**, 155005 (2009).
[10] L. Kang, Q. Zhao, H. Zhao, and J. Zhou, Opt. Express **16**, 17269 (2008).
[11] Y. Poo, R. X. Wu, G. H. He, and P. Chen, Appl. Phys. Lett. **96**, 161902 (2010).
[12] F. Zhang, L. Kang, Q. Zhao, J. Zhou, X. Zhao, and D. Lippens, Opt. Express **17**, 4360 (2009).
[13] D. Shrekenhamer, W.-C. Chen, and W. J. Padilla, Phys. Rev. Lett. **110**, 177403 (2013).
[14] Q. Zhao, L. Kang, B. Du, B. Li, J. Zhou, H. Tang, X. Liang, and B. Zhang, Appl. Phys. Lett. **90**, 011112 (2007).
[15] T. Nesimoglu and C. Sabah, IEEE Trans. Circuits Syst. II, Exp. Briefs **63**, 89 (2016).
[16] D. Wang, L. Ran, H. Chen, M. Mu, J. A. Kong, and B. I. Wu, Appl. Phys. Lett. **91**, 164101 (2007).
[17] H. Chen, B. I. Wu, L. Ran, T. M. Grzegorczyk, and J. A. Kong, Appl. Phys. Lett. **89**, 053509 (2006).
[18] J. F. Wang, S. B. Qu, H. Ma, J. Zhang, and H. Du, IEEE Mtt-S International Microwave Workshop Series on Advanced Materials and Processes for Rf and Thz Applications, 2015.
[19] C. Sabah, Prog. Electromagn. Res. B **22**, 341 (2010).
[20] J. Wang, S. Qu, J. Zhang, H. Ma, Y. Yang, C. Gu, X. Wu, and Z. Xu, Prog. Electromagn. Res. Lett. **6**, 35 (2009).
[21] J. Wang, S. Qu, Y. Yang, H. Ma, X. Wu, and Z. Xu, Appl. Phys. Lett. **95**, 014105 (2009).
[22] E. Ekmekci, K. Topalli, T. Akin, and G. Turhansayan, Opt. Express **17**, 16046 (2009).
[23] H. Zhou, C. Wang, and H. Peng, J. Mater. Sci. Mater. Electron. **27**, 2534 (2016).
[24] A. Sarkhel, D. Mitra, and S. R. B. Chaudhuri, Appl. Phys. A **122**, 1 (2016).
[25] H. X. Xu, G. M. Wang, C. X. Zhang, Q. Liu, Z. M. Xu, X. Chen, and D. L. Zhai, Phot. Nano. Fund. Appl. **11**, 15 (2013).
[26] O. Yurduseven, A. E. Yilmaz, and G. Turhan-Sayan, Electron. Lett. **47**, 1381 (2011).
[27] H. Chen, L. Ran, J. Huangfu, X. Zhang, K. Chen, T. M. Grzegorczyk, and J. A. Kong, J. Appl. Phys. **96**, 5338 (2004).
[28] J. H. Lim and S. S. Kim, J. Magn. **21**, 187 (2016).
[29] A. Ourir and H. H. Ouslimani, Appl. Phys. Lett. **98**, 113505 (2011).
[30] N. T. Tung, V. T. T. Thuy, W. P. Jin, J. Y. Rhee, and Y. P. Lee, J. Appl. Phys. **107**, 023530 (2010).
[31] J. Zhou, T. Koschny, L. Zhang, and G. Tuttle, Appl. Phys. Lett. **88**, 221103 (2006).
[32] J. Zhou, E. N. Economon, T. Koschny, and C. M. Soukoulis, Opt. Lett. **31**, 3620 (2006).
[33] V. M.Shalaev, W. Cai, U. Chettiar, H. K. Yuan, A. K. Sarychev, V. P. Drachev, and A. V. Kildishev, Front. Opt., 2005.
[34] D. Ye, K. Chang, L. Ran, and H. Xin, Nat Commun **5**, 5841 (2014).
[35] I. Bahl and P. Bhartia, Microwave Solid State Circuit Design. Wiley, 2003.
[36] X. Chen, T. M. Grzegorczyk, B. I. Wu, P. J. Jr, and J. A. Kong, Phys. Rev. E **70**, 811 (2004).
[37] S. Ghosh and A. Chakrabarty, J. Electrostat. **66**, 142 (2008).
[38] O. Sydoruk, E. Tatartschuk, E. Shamonina, and L. Solymar, J. Appl. Phys. **105**, 014903 (2009).